Sensing the wavefront of x-ray free-electron lasers using aerosol spheres

N. Duane Loh[1], Dmitri Starodub[1], Lukas Lomb[2], Christina Y. Hampton[1], Andrew V. Martin[3], Raymond G. Sierra[1], Anton Barty[4], Andrew Aquila[5], Joachim Schulz[5], Jan Steinbrener[2], Robert L. Shoeman[2], Stephan Kassemeyer[2], Christoph Bostedt[6], John Bozek[6], Sascha W. Epp[7], Benjamin Erk[7], Robert Hartmann[8], Daniel Rolles[7], Artem Rudenko[7], Benedikt Rudek[7], Lutz Foucar[2,7], Nils Kimmel[9], Georg Weidenspointner[9,10], Guenter Hauser[9,10], Peter Holl[8], Emanuele Pedersoli[11], Mengning Liang[4], Mark S. Hunter[12], Lars Gumprecht[4], Nicola Coppola[5], Cornelia Wunderer[13], Heinz Graafsma[13], Filipe R.N.C. Maia[14], Tomas Ekeberg[15], Max Hantke[15], Holger Fleckenstein[4], Helmut Hirsemann[13], Karol Nass[4], Thomas A. White[4], Herbert J. Tobias[16], George R. Farquar[12], W. Henry Benner[12], Stefan Hau-Riege[12], Christian Reich[8], Andreas Hartmann[8], Heike Soltau[8], Stefano Marchesini[14], Sasa Bajt[13], Miriam Barthelmess[13], Lothar Strueder[9], Joachim Ullrich[17], Philip Bucksbaum[1], Matthias Frank[12], Ilme Schlichting[2], Henry N. Chapman[4] and Michael J. Bogan[1].

[1]*PULSE Institute, SLAC National Accelerator Laboratory, 2575 Sand Hill Road, Menlo Park, CA 94025 USA.*
[2]*Max-Planck-Institut für medizinische Forschung, Jahnstr. 29, 69120 Heidelberg, Germany.*
[3]*ARC Centre of Excellence for Coherent X-ray Science, School of Physics, University of Melbourne, Parkville, Victoria 3010, Australia.*
[4]*Center for Free-Electron Laser Science, DESY, Notkestraße 85, 22607 Hamburg, Germany.*
[5]*European XFEL GmbH, Notkestraße 85, 22607 Hamburg, Germany.*
[6]*SLAC National Accelerator Laboratory, 2575 Sand Hill Road, Menlo Park, CA 94025 USA.*
[7]*Max Planck Advanced Study Group, CFEL, Notkestraße 85, 22607 Hamburg, Germany.*
[8]*PNSensor GmbH, Römerstr. 28, 80803 München, Germany.*
[9]*Max-Planck-Institut Halbleiterlabor, Otto-Hahn-Ring 6, 81739 München, Germany.*
[10]*Max-Planck-Institut für extraterrestrische Physik, Giessenbachstrasse, 85741 Garching, Germany.*
[11]*Elettra-Sincrotrone Trieste, SS 14 - km 163.5 in AREA Science Park, 34149 Basovizza, Trieste, Italy.*
[12]*Lawrence Livermore National Laboratory, 7000 East Avenue, Livermore, CA 94551 USA.*
[13]*Photon Science, DESY, Notkestraße 85, 22607 Hamburg, Germany.*
[14]*Lawrence Berkeley National Laboratory, 1 Cyclotron Road, Berkeley, CA 94720, USA.*
[15]*Laboratory of Molecular Biophysics, Uppsala University, Husargatan 3 (Box 596), SE-751 24 Uppsala, Sweden.*
[16]*Cornell University, Division of Nutritional Sciences, Savage Hall, Ithaca, NY 14853, USA.*
[17]*Physikalisch-Technische Bundesanstalt, Bundesallee 100, D-38116 Braunschweig, Germany.*

duaneloh@slac.stanford.edu

Abstract: Characterizing intense, focused x-ray free electron laser (FEL) pulses is crucial for their use in diffractive imaging. We describe how the distribution of average phase tilts and intensities on hard x-ray pulses with peak intensities of 10^{21} W/m^2 can be retrieved from an ensemble of diffraction patterns produced by 70 nm-radius polystyrene spheres, in a manner that mimics wavefront sensors. Besides showing that an adaptive geometric correction may be necessary for diffraction data from randomly injected sample sources, our paper demonstrates the possibility of collecting statistics on structured pulses using only the diffraction patterns they generate and highlights the imperative to study its impact on single-particle diffractive imaging.

OCIS codes: 140.2600 Free-electron lasers (FELs), 110.7440 X-ray imaging, 010.7350 Wavefront sensing, 030.6600 Statistical optics, 050.1940 Diffraction, 110.1650 Coherence imaging, 110.1758 Computational imaging.

References and links

1. P Emma, R Akre, J Arthur, Richard M Bionta, C Bostedt, J Bozek, A Brachmann, Philip H. Bucksbaum, Ryan Coffee, F J Decker, Y Ding, D Dowell, S Edstrom, A Fisher, J Frisch, S Gilevich, J Hastings, G Hays, Ph Hering, Z Huang, R Iverson, H Loos, M. Messerschmidt, A Miahnahri, S. Moeller, Heinz-Dieter Nuhn, D Pile, D Ratner, J Rzepiela, D Schultz, T Smith, Peter Stefan, H Tompkins, J Turner, J Welch, W White, J Wu, G Yocky, and John N Galayda. "First lasing and operation of an angstrom-wavelength free-electron laser". Nature Photonics **4**, 641–647 (2010).
2. N D Loh, M J Bogan, Veit Elser, Anton Barty, Sébastien Boutet, Saša Bajt, Janos Hajdu, Tomas Ekeberg, F R N C Maia, J Schulz, M M Seibert, B Iwan, N Tîmneanu, S Marchesini, I Schlichting, Robert L Shoeman, L Lomb, M Frank, M Liang, and Henry N Chapman. "Cryptotomography: Reconstructing 3D Fourier Intensities from Randomly Oriented Single-Shot Diffraction Patterns". Phys. Rev. Lett. **104**, 25501 (2010).
3. Michael J Bogan, Sébastien Boutet, Henry N Chapman, S Marchesini, Anton Barty, W Henry Benner, U Rohner, Matthias Frank, S P Hau-Riege, Saša Bajt, Bruce W Woods, M M Seibert, Bianca Iwan, Nicusor Timneanu, Janos Hajdu, and Joachim Schulz. "Aerosol Imaging with a Soft X-ray Free Electron Laser". Journal of Aerosol Science and Technology **44(3)**, 1–6 (2010).
4. M Marvin Seibert, Tomas Ekeberg, Filipe R N C Maia, Martin Svenda, Jakob Andreasson, Olof Jonsson, Duško Odic, Bianca Iwan, Andrea Rocker, Daniel Westphal, Max Hantke, Daniel P DePonte, Anton Barty, Joachim Schulz, Lars Gumprecht, Nicola Coppola, Andrew Aquila, Mengning Liang, Thomas A White, Andrew Martin, Carl Caleman, Stephan Stern, Chantal Abergel, Virginie Seltzer, Jean-Michel Claverie, Christoph Bostedt, John D Bozek, Sébastien Boutet, A Alan Miahnahri, Marc Messerschmidt, Jacek Krzywinski, Garth J. Williams, Keith O Hodgson, Michael J Bogan, Christina Y Hampton, Raymond G Sierra, Dmitri Starodub, Inger Andersson, Saša Bajt, Miriam Barthelmess, John C H Spence, Petra Fromme, Uwe Weierstall, Richard Kirian, Mark Hunter, R Bruce Doak, Stefano Marchesini, Stefan P Hau-Riege, Matthias Frank, Robert L Shoeman, Lukas Lomb, Sascha W Epp, Robert Hartmann, Daniel Rolles, Artem Rudenko, Carlo Schmidt, Lutz Foucar, Nils Kimmel, Peter Holl, Benedikt Rudek, Benjamin Erk, André Hömke, Christian Reich, Daniel Pietschner, Georg Weidenspointner, Lothar Strüder, Günter Hauser, Hubert Gorke, Joachim Ullrich, Ilme Schlichting, Sven Herrmann, Gerhard Schaller, Florian Schopper, Heike Soltau, Kai-Uwe Kühnel, Robert Andritschke, Claus-Dieter Schröter, Faton Krasniqi, Mario Bott, Sebastian Schorb, Daniela Rupp, Marcus Adolph, Tais Gorkhover, Helmut Hirsemann, Guillaume Potdevin, Heinz Graafsma, Björn Nilsson, Henry N Chapman, and Janos Hajdu. "Single mimivirus particles intercepted and imaged with an X-ray laser". Nature (London) **470(7332)**, 78–81 (2011).
5. Stephan Kassemeyer, Jan F. Steinbrener, Lukas Lomb, Eisabeth Hartmann, Andrew Aquila, Anton Barty, Andrew V Martin, Christina Y Hampton, Saša Bajt, Miriam Barthelmess, Thomas R M Barends, Christoph Bostedt, Mario Bott, John D Bozek, Nicola Coppola, Max Cryle, Daniel P DePonte, R Bruce Doak, Sascha W Epp, Benjamin Erk, Holger Fleckenstein, Lutz Foucar, Heinz Graafsma, Lars Gumprecht, Andreas Hartmann, Robert Hartmann, Günter Hauser, Helmut Hirsemann, André Hömke, Peter Holl, Olof Jonsson, Nils Kimmel, Faton Krasniqi, Mengning Liang, Filipe R N C Maia, Stefano Marchesini, Karol Nass, Christian Reich, Daniel Rolles, Benedikt Rudek, Artem Rudenko, Carlo Schmidt, Joachim Schulz, Robert L Shoeman, Raymond G Sierra, Heike Soltau, John C H Spence, Dmitri Starodub, Francesco Stellato, Stephan Stern, Gunter Stier, Martin Svenda, Georg Weidenspointner, Uwe Weierstall, Thomas A White, Cornelia B Wunderer, Matthias Frank, Henry N Chapman, Joachim Ullrich, Lothar Strüder, Michael J Bogan, and Ilme Schlichting. "Femtosecond free-electron laser x-ray diffraction data sets for algorithm development". Opt. Express **20(4)**, 4149–4158 (2012).

6. N D Loh, C Y Hampton, A V Martin, Dmitri Starodub, R G Sierra, Anton Barty, Andrew Aquila, J Schulz, L Lomb, Jan F. Steinbrener, Robert L Shoeman, Stephan Kassemeyer, C Bostedt, J Bozek, S W Epp, B Erk, R Hartmann, D Rolles, A Rudenko, B Rudek, L Foucar, N Kimmel, G Weidenspointner, G Hauser, P Holl, E Pedersoli, M Liang, M S Hunter, L Gumprecht, N Coppola, C Wunderer, H Graafsma, F R N C Maia, Tomas Ekeberg, M Hantke, H Fleckenstein, H Hirsemann, K Nass, T A White, H J Tobias, G R Farquar, W H Benner, S P Hau-Riege, C Reich, A Hartmann, H Soltau, S Marchesini, Saša Bajt, M Barthelmess, Philip H. Bucksbaum, K O Hodgson, L Strüder, J Ullrich, M Frank, I Schlichting, Henry N Chapman, and M J Bogan. "Fractal morphology, imaging and mass spectrometry of single aerosol particles in flight". Nature (London) **486(7404)**, 513–517 (2012).
7. J. Chalupsky, L. Juha, J Kuba, J Cihelka, V Hajkova, S Koptyaev, J Krása, A Velyhan, Magnus Bergh, Carl Caleman, Janos Hajdu, Richard M Bionta, Henry N Chapman, S P Hau-Riege, R A London, M Jurek, J Krzywinski, R Nietubyc, J B Pelka, R Sobierajski, J Meyer-ter Vehn, A Tronnier, K Sokolowski-Tinten, N Stojanovic, K Tiedtke, S Toleikis, T Tschentscher, H. Wabnitz, and U. Zastrau. "Characteristics of focused soft X-ray free-electron laser beam determined by ablation of organic molecular solids". Opt. Express **15(10)**, 6036–6043, (2007).
8. J. Chalupsky, P Bohacek, V Hajkova, S P Hau-Riege, P. A. Heimann, L. Juha, J Krzywinski, M. Messerschmidt, S. P. Moeller, B. Nagler, M. Rowen, W F Schlotter, M. L. Swiggers, and J. J. Turner. "Comparing different approaches to characterization of focused X-ray laser beams". Nuclear Instruments and Methods in Physics Research A **631**, 130–133 (2011).
9. Stefan P Hau-Riege, R London, Michael J Bogan, and Henry N Chapman. "Damage-resistant single-pulse optics for x-ray free electron lasers". Proceedings of SPIE (2007).
10. Simon Rutishauser, Liubov Samoylova, Jacek Krzywinski, Oliver Bunk, Jan Grunert, Harald Sinn, Marco Cammarata, David M Fritz, and Christian David. "Exploring the wavefront of hard X-ray free-electron laser radiation". Nature Communications **3(947)**, 1–6 (2012).
11. S Le Pape, Ph. Zeitoun, M Idir, P Dhez, J Rocca, and M François. "Electromagnetic-Field Distribution Measurements in the Soft X-Ray Range: Full Characterization of a Soft X-Ray Laser Beam". Phys. Rev. Lett. **88(18)**, 183901 (2002).
12. B Flöter, P Juranić, S Kapitzki, B Keitel, Klaus Mann, Elke Plönjes, Bernd Schafer, and K Tiedtke. "EUV Hartmann sensor for wavefront measurements at the Free-electron LASer in Hamburg". New Journal of Physics **12**, 083015 (2010).
13. M Idir, P Mercère, MH Modi, G Dovillaire, Xavier Levecq, Samuel Bucourt, Lionel Escolano, and Paul Sauvageot. "X-ray active mirror coupled with a Hartmann wavefront sensor". Nuclear Inst and Methods in Physics Research A **616(2-3)**, 162–171 (2010).
14. John D Bozek. "AMO instrumentation for the LCLS X-ray FEL". The European Physical Journal-Special Topics **169**, 129–132 (2009).
15. W Henry Benner, Michael J Bogan, U Rohner, Sébastien Boutet, Bruce W Woods, and Matthias Frank. "Non-destructive characterization and alignment of aerodynamically focused particle beams using single particle charge detection". Aerosol Science **39**, 917–928 (2008).
16. Michael J Bogan, W Henry Benner, Sébastien Boutet, U Rohner, M Frank, Anton Barty, M M Seibert, F R N C Maia, S Marchesini, Saša Bajt, Bruce W Woods, Vincent Riot, S P Hau-Riege, Martin Svenda, Erik Marklund, Eberhard Spiller, Janos Hajdu, and Henry N Chapman. "Single Particle X-ray Diffractive Imaging". Nano Letters **8(1)**, 310–316 (2008).
17. L Strüder, S Epp, D Rolles, and R Hartmann. "Large-format, high-speed, X-ray pnCCDs combined with electron and ion imaging spectrometers in a multipurpose chamber for experiments at 4th generation light sources". Nuclear Instruments and Methods in Physics Research A **614**, 483–496 (2010).
18. Anton Barty, R Soufli, T McCarville, Sherry L. Baker, Michael J. Pivovaroff, P Stefan, and Richard M Bionta. "Predicting the coherent X-ray wavefront focal properties at the Linac Coherent Light Source (LCLS) X-ray free electron laser". Opt. Express **17(18)**,15508–15519 (2009).
19. IA Vartanyants, A Singer, AP Mancuso, OM Yefanov, A. Sakdinawat, Y. Liu, E. Bang, Garth J. Williams, G. Cadenazzi, B. Abbey, H Sinn, D Attwood, K A Nugent, Edgar Weckert, T Wang, D Zhu, B Wu, C Graves, A Scherz, J. J. Turner, W F Schlotter, M. Messerschmidt, J Lüning, Y Acremann, P Heimann, D C Mancini, V Joshi, Jacek Krzywinski, R Soufli, M Fernandez-Perea, S P Hau-Riege, A G Peele, Y Feng, Oleg Krupin, S. Moeller, and W. Wurth. "Coherence Properties of Individual Femtosecond Pulses of an X-Ray Free-Electron Laser". Phys. Rev. Lett. **107(14)**, 144801 (2011).
20. Lukas Lomb, Thomas R M Barends, Stephan Kassemeyer, Andrew Aquila, Sascha W Epp, Benjamin Erk, Lutz Foucar, Robert Hartmann, Benedikt Rudek, Daniel Rolles, Artem Rudenko, Robert L Shoeman, Jakob Andreasson, Saša Bajt, Miriam Barthelmess, Anton Barty, Michael J Bogan, Christoph Bostedt, John D Bozek, Carl Caleman, Ryan Coffee, Nicola Coppola, Daniel P DePonte, R Bruce Doak, Tomas Ekeberg, Holger Fleckenstein, Petra Fromme, Maike Gebhardt, Heinz Graafsma, Lars Gumprecht, Christina Y Hampton, Andreas Hartmann, Günter Hauser, Helmut Hirsemann, Peter Holl, James M Holton, Mark S Hunter, Wolfgang Kabsch, Nils Kimmel, Richard A Kirian, Mengning Liang, Filipe R N C Maia, Anton Meinhart, Stefano Marchesini, Andrew V Martin, Karol Nass, Christian Reich, Joachim Schulz, M Marvin Seibert, Raymond G Sierra, Heike Soltau, John

C H Spence, Jan F. Steinbrener, Francesco Stellato, Stephan Stern, Nicusor Timneanu, Xiaoyu Wang, Georg Weidenspointner, Uwe Weierstall, Thomas A White, Cornelia B Wunderer, Henry N Chapman, Joachim Ullrich, Lothar Strüder, and Ilme Schlichting. "Radiation damage in protein serial femtosecond crystallography using an x-ray free-electron laser". Phys. Rev. B **84**, 214111 (2011).
21. Ne-Te Duane Loh and Veit Elser. "Reconstruction algorithm for single-particle diffraction imaging experiments". Phys. Rev. E **80**, 6705 (2009).
22. Peter Schwander, Dimitrios Giannakis, Chun Hong Yoon, and Abbas Ourmazd. "The symmetries of image formation by scattering. II. Applications". Opt. Express **20(12)**, 12827–12849 (2012).

1. Introduction

Diffractive imaging experiments with x-ray free-electron lasers (FELs) aim to expose individual weakly scattering samples to a brief and intense focused x-ray pulse, scattering photons appreciably before the onset of radiation damage. For such purposes hard x-ray pulses, such as those produced by the Linac Coherent Light Source (LCLS) [1] with peak powers reaching 40 GW, are focused onto spots that are several microns across or smaller. Particles are randomly delivered [2, 3, 4, 5, 6] into these tightly focused x-ray pulses (Fig. 1), producing a diffraction pattern each time pulse and particle interact. Profiling such focused pulses critically determines where these particles should be injected in order to maximize and properly interpret their diffraction signal.

In principle, to study these intense, hard x-ray FEL pulses one could consider using ablation imprints [7, 8, 9], scintillation crystals, grating interferometers [10] or x-ray sensitive Hartmann wavefront sensors [11, 12, 13]. However, the extraordinarily high peak intensities of FEL pulses near their small foci have made this extremely challenging, either because of the potential damage to such instruments or the difficulty in interpreting their measurements or both. Although absolute photon intensities can be extrapolated by measuring strongly attenuated pulses, the attenuators may potentially distort finer structures in unattenuated pulse wavefronts.

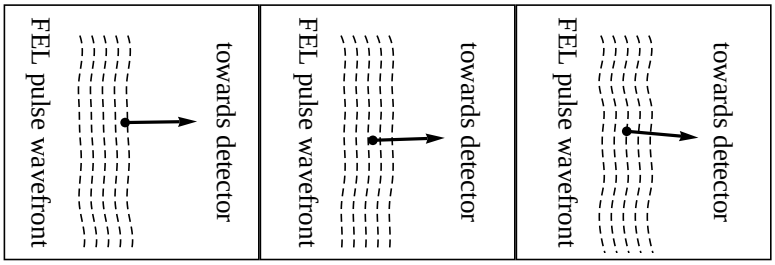

Fig. 1. Phase tilts (wavefront shape) of FEL pulses (dashed wavy lines) cause the centers of diffraction patterns to diverge. The disks in these panels represent polystyrene spheres that are randomly injected into the page to separately intercept three different FEL pulses. The centers of resultant diffraction patterns travel along directions (black arrows) perpendicular to the beam's wavefront towards the detector, as indicated by the arrows.

2. Description of technique

This paper demonstrates how a diffractive imaging setup with randomly injected polystyrene spheres can be sensitive to the shape of an FEL pulse's wavefront and its intensity profile even at peak intensities of 10^{21} W/m^2 (exceeding 1.5 kJ/cm^2 per pulse). Furthermore, such measurements require little additional effort beyond routine calibration already performed to optimize sample injection. Only several minutes of data collection are needed given our aerosol injection rate and LCLS's designed 120 Hz pulse rate. These measurements also produce direct

estimates on the extent of data correction necessary for samples that are injected into the same region of the stream of structured x-ray pulses (Fig. 1), without the need to infer this information from wavefront profiles collected using conventional sensors if they become available for x-ray FELs. Furthermore, we only require a sample change in the aerosol injector without breaking the high-vacuum in the experiment chamber to insert additional diagnostic instruments.

The working principle of our technique is analogous to a Hartmann wavefront sensor with spheres acting as randomly positioned, disposable lenses. Each injected sphere probes a local region of the FEL pulse that it intercepts: offsets in the center of the resultant diffraction pattern indicate the pulse's local wavefront shape or, equivalently, phase tilt (Fig. 1); the brightness of the pattern indicates the pulse's local intensity. These measurements are averaged over the finite depth of the pulse stream's focus, equivalent to the spot diameter of the spray of spheres (circle in Fig. 2). The character of the average FEL pulse can be reconstructed when many single sphere measurements are combined.

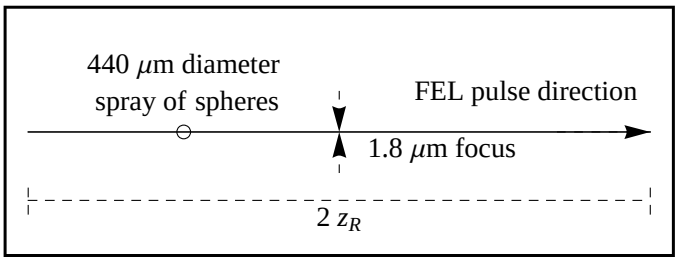

Fig. 2. Sample-beam interaction region. The image is centered on the FEL pulse focus (1.8 μm pulse waist) and spans twice the pulse's nominal Rayleigh length $z_R = 10$ mm. FEL pulses traveled along the solid horizontal line towards the right; random spray of polystyrene spheres was injected into the page at the empty circle. This circle represents the interaction region where the spheres were illuminated by the line of pulses (typified by Fig. 1), whose location was known to within z_R of the nominal pulse focus.

3. Experimental demonstration

The diffractive imaging experiment was performed at the Atomic Molecular and Optical Science beamline [14] at the LCLS. X-ray pulses were produced at 60 Hz by the FEL with an average pulse energy of 2.7 mJ (4.8% pulse-to-pulse r.m.s. variation) while spanning a FWHM pulse duration of approximately 150 fs (measured from the lasing electron bunch). These pulses contained 1.2 keV photons (wavelength 1.0 nm, with 0.28% r.m.s. pulse-to-pulse variation in its average) thus providing an average of 1.4×10^{13} photons per pulse, focused using Kirkpatrick-Baez mirrors to a 10 μm^2 spot. Polystyrene spheres (70 nm average radius) in solution were nebulized and injected into the FEL focus with a differentially-pumped aerodynamic lens stack [15, 16, 3]. These spheres were randomly irradiated by FEL pulses in a narrow range of defocus planes spanning only 4.4% of the FEL pulse's Rayleigh length (Fig. 2). Diffraction patterns were recorded by a 1024×1024-pixel pnCCD x-ray detector [17] comprising 75×75 μm^2 pixels (Fig. 3). The detector readout was recorded at 60 Hz, with one pattern per pulse whether or not it encountered an injected particle. From these, a software implemented intensity filter selected background-subtracted patterns that contained scattering signal (*hits*), which included single and multiple coincident spheres. More than 2000 hits were collected with 625 patterns from single spheres. Patterns from multiple coincident spheres were eliminated by inspecting fits to single sphere diffraction intensities. Only five single-sphere patterns were excluded before arriving at these 625 patterns because detector readout saturation in these five caused poor

fits to (2). Radiation damage to the polystyrene spheres during illumination by these ultrashort pulses was undetectable at low resolution.

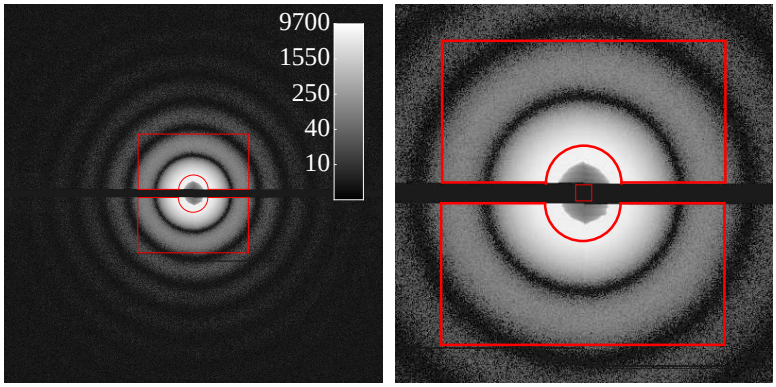

Fig. 3. A centered diffraction image from a single polystyrene sphere. Left: logarithm of the detector counts for a typical diffraction pattern with 1024×1024 pixels (counts in grayscale bar). Right: magnified view of the central portion of the pattern. Candidate centers of the pattern were restricted to the 17×17 pixel box in the middle of the detector, selecting for the center about which the intensities in the two 'u-shaped' regions above and below (outlined in red) appear most azimuthally-symmetric. The horizontal band in the middle of the diffraction pattern, which includes two quasi-semicircular regions, marks the gap between the two detector panels through which unscattered photons pass.

The local phase tilt (wavefront shape) on a pulse that each sphere randomly intercepts caused the resultant diffraction pattern to translate (Fig. 1). Each pattern was centered by identifying the central pixel about which the pattern was most azimuthally symmetric. Azimuthally averaged intensities $I(q_c)$ around each candidate center c were computed then scored against the original two-dimensional pattern assuming such a center

$$I(\mathbf{q}_c):\ \mathrm{argmax}_c \left[\sum_{|\mathbf{q}_c|=q_c} \log\left(I(q_c)\right) \log\left(I(\mathbf{q}_c)\right) \right] . \tag{1}$$

The candidate center with the highest score was taken to be the correct central pixel. The logarithm of the diffraction intensities were used to increase the sensitivity of this scoring over a wider dynamic range of intensities. This scoring was done for intensities at small diffraction angles, where each sphere's high-resolution deviation from sphericity is least manifest, while constraining the gap between the two detector halves to be 21 pixels (as estimated from maximizing the fringe visibility in the radial average of the brightest, centered sphere diffraction patterns). An exhaustive search for candidate centers c was restricted to pixels in a 17×17-pixel region centered on the nominal center. Centered patterns of single spheres were expected to fit the spherically symmetric scalar diffraction intensity distribution

$$I_{\mathrm{sph}}(q,r) = I_0 \left[\frac{\sin(qr) - qr\cos(qr)}{(qr)^3} \right]^2 , \tag{2}$$

where the magnitude of the spatial frequency $\mathbf{q}$ is denoted as q, radius of a polystyrene sphere as r, and the fit parameter I_0 is related to the forward scattering cross section and incident photon fluence. Knowing both r and I_0 from fits for each pattern also gives us the incident photon fluence I_{inc} on each sphere.

The detector readout of a single sphere diffraction pattern at spatial frequency $q = 0$ is expected to be:

$$I_{\mathrm{sph}}(0,r) = I_{\mathrm{inc}} G_{\mathrm{det}} Q_{\mathrm{eff}} r_e^2 \Delta\Omega \left(\overline{f} N_{\mathrm{A}} \rho_{\mathrm{PSL}} 4\pi r^3 / (3M_{\mathrm{PSL}})\right)^2 , \quad (3)$$

where the density of polystyrene ρ_{PSL}, provided by the sphere manufacturer, is 1.05 g/cm^3; N_{A} is Avogadro's constant; M_{PSL} is the molar weight of polystyrene monomers (C_8H_8), 104 g/mol; $\overline{f}$ is the average scattering factor of polystyrene monomers for 1.2 keV radiation, 58.3; r_e is the classical electron radius, 2.8×10^{-15} m; $\Delta\Omega$ is the solid angle subtended by each detector pixel, 1.1×10^{-8} steradians; G_{det} is the detector's gain, 7 counts per photon; and Q_{eff} is its quantum efficiency for 1.2 keV photons, 0.9 efficiency.

We calibrated the average radius of our polystyrene spheres against a separate differential mobility analyzer (DMA) measurement of polystyrene spheres similar to those used for our diffraction data. The radii measurement from DMA was considerably larger than that nominally specified by the manufacturer, PostNova Analytics (Germany), who reported a radius of 68.5 nm spheres and a coefficient of variance of 2.3%. Our DMA radii measurement, 69.6 $\pm$ 3.4 nm, was used for calibration because of its recency and inclusion of possible post-manufacture growth factors.

4. Visualizing experimental data

Pulse-to-pulse fluctuations in the average photon wavelength (0.5% r.m.s. variation) were accounted for when fitting each diffraction pattern, as were fluctuations in total pulse energies (4.8% r.m.s. variation) measured using the UV fluorescence generated from calibrated nitrogen gas detectors upstream of the interaction region [1]. Incident fluences I_{inc} from fitting Eq. (2) were normalized using this fluorescence readout such that all pulses had the same total energy equal to the highest measured pulse energy. The uncertainty in FEL-sphere interaction region introduced less than 0.1% uncertainty in each sphere's determined radius, and hence less than 0.6% in the local incident photon fluence I_{inc}. Since both pattern centering and sphere sizing depended primarily on low-resolution features of the spheres, we did not correct for errors arising from higher resolution non-sphericities in our polystyrene spheres.

The measured translations necessary for pattern-centering and incident fluence from fits to sphere diffraction patterns are combined in Fig. 4, where pattern translations at the detector were converted to angular deviations from the nominal center of the pulse focus. The abrupt bottom and right edges of the contour plot in Fig. 4 were from pulse truncation by beam guards on the Kirkpatrick-Baez focusing mirrors. The number of patterns that suffered each deviation are superimposed on Fig. 4, which show the distribution of phase tilts on the average FEL pulse over a 440 μm depth of focus (Fig. 2).

5. Discussion

The 0.5 mrad r.m.s. variation in divergence angle of the sphere patterns (Fig. 4) is comparable to the focused pulse's estimated divergence angle of 0.7 mrad. Ref [1] notes that at hard x-ray wavelengths the pulses from the LCLS should only show a r.m.s. centroid variation which is 10-20% of the beam size. The larger angular deviations we measured suggest that either our polystyrene spheres were injected away from the pulse foci where there was substantial phase curvature or that there were residual phase curvature or phase tilt fluctuations at these foci (circular region in Fig. 2). These two cases can be distinguished, in further studies, by measuring distributions like those in Fig. 4 while longitudinally stepping through the pulse foci. Until we can ascertain the positions of our spheres when they were illuminated by the pulses, we will not have direct spatial and temporal measurements on these pulses. However, convex

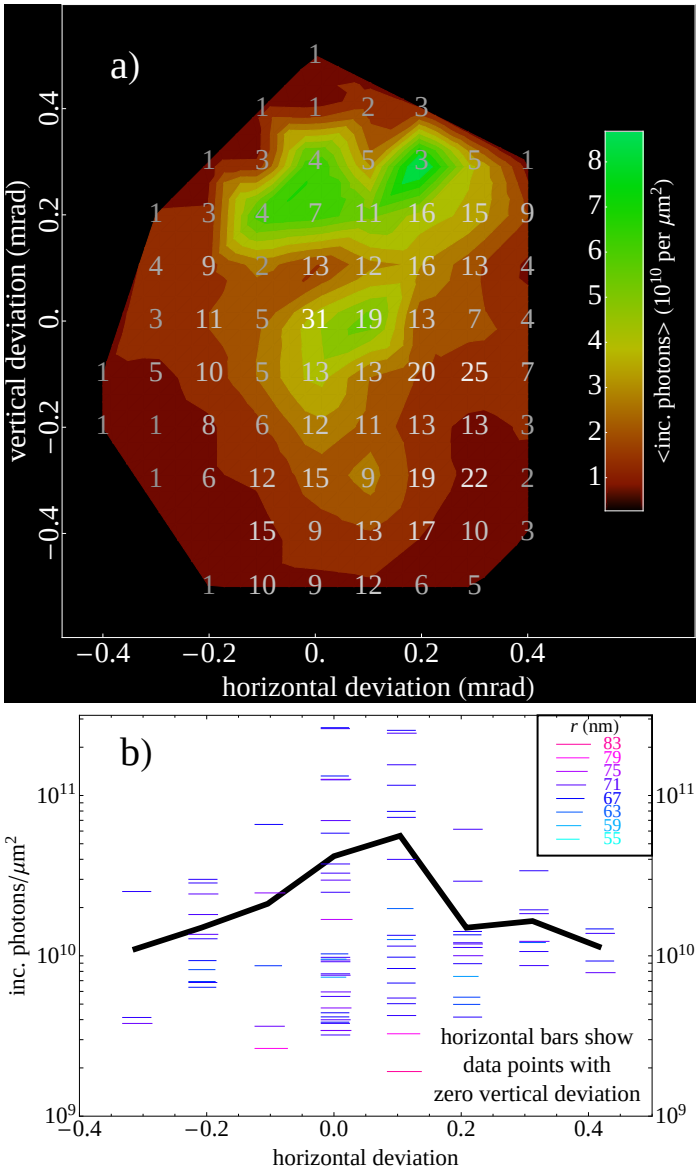

Fig. 4. Translations of 625 sphere diffraction patterns and their local incident pulse fluence. (a) Interpolated contour plot shows the average incident photon fluence for patterns that suffer the same translation or, equivalently, angular deviation; this is superimposed with the number of patterns with each translation. The zero deviation position was chosen to be the one with most patterns. (b) Photon fluence for patterns with zero vertical deviation. Each horizontal bar represents a pattern, whose sphere's radius r is shown with the bar's length and color. The thick black line charts their average fluence.

wavefronts are exceptions since we can relate each sphere's transverse position at illumination to a unique translation of its diffraction pattern at the detector.

While Fig. 4a averages over the experimental conditions to which we subjected our spheres, the distribution of data that comprise these averages (Fig. 4b) are a clearer indication of how

samples will perform under similar conditions. We observed a considerable fluence variation between data points in Fig. 4b, which did not result from temporal fluctuations in total pulse energy since this effect was normalized away. Nor do the modest variations in sphere radii r suggest that systematic errors from fitting r in (2) can account for these large fluence variations. Although these fluence variations may arise from non-convex pulse wavefronts, potential connections with the pulses' pointing stability could also be investigated by including pulse-to-pulse measurements of beamline parameters.

Nevertheless, the distribution in Fig. 4a differs considerably from that produced by an azimuthally-symmetric spherical Gaussian beam near its focus. Similar spatial deviations were predicted to arise from the figure and finish of the mirrors used to direct the x-ray pulses into the imaging chamber [18] and were also observed (in addition to pulse-to-pulse variations) at the FLASH facility when Hartmann sensors measured the defocused, attenuated extreme-ultraviolet FEL pulses [12].

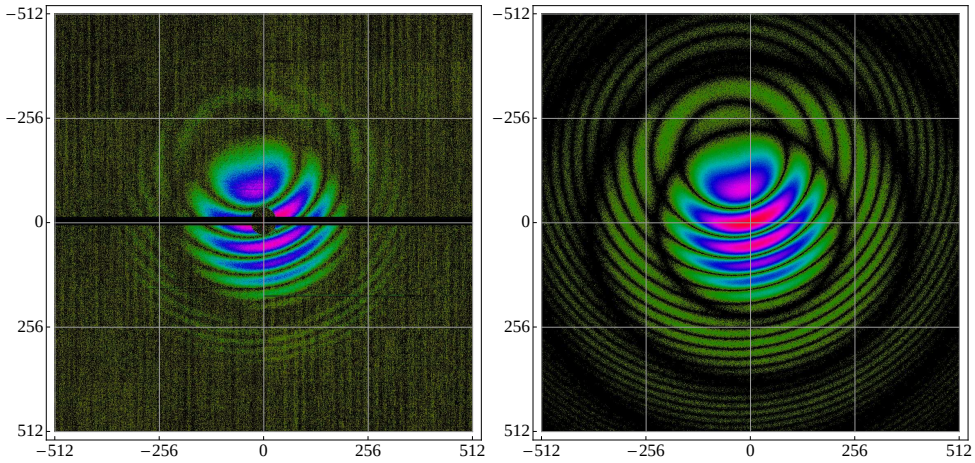

Fig. 5. An experimental two-sphere diffraction pattern on a 1024×1024 pixel detector (left) and its simulated fit (right). The spheres in the simulation both had radii of 30 nm, and were separated by $\{140, 35\}$ nm transversely and 8.0 μm longitudinally to the pulse propagation direction.

Indirect measurements on the pulses from Fig. 4 can improve both the FEL optics and imaging experiments. For example, incremental adjustments to bendable mirrors used to focus the pulses [13] can be guided by maximizing the absolute photon fluence measurements and/or narrowing the distribution of phase tilts in Fig. 4. Unlike profiling measurements that probe the wavefront away from where samples will be injected, Fig. 4 directly captures the distribution of photon fluence and phase tilts applicable to samples injected under similar conditions. Repeating the measurements in Fig. 4 as a function of time and across different longitudinal positions of the FEL pulse focus are under development, as is the possibility of extracting information about pulses when they illuminate multiple aerosol spheres (Fig. 5), similar to two-point correlation studies on the FEL pulses using pinholes [19]. These statistics affect radiation damage studies with x-ray FELs [20].

6. Conclusions

The adaptive centering of individual patterns has been overlooked in the literature on single-particle three-dimensional diffractive imaging. Such corrective centering, when necessary, reduces resolution loss from translational blurring. This issue is exacerbated when imaging

nanoparticles smaller than the spheres studied in this paper. For such nanoparticles, x-ray pulses will likely be focused to smaller foci to attain higher peak pulse intensities: this also increases the pulse's wavefront curvature and potentially exaggerates the translations compared to those in Fig. 4. The diffraction patterns will likely be noisier than those typified by Fig. 3 and hence more challenging to center. These serious concerns urge an understanding of how the spatial and temporal structure of FEL pulses will impact diffractive imaging with x-ray FELs, especially in reconstruction schemes that integrate many noisy, incomplete single-particle diffraction data [21, 22].

Acknowledgements

Experiments were carried out at the LCLS, a national user facility operated by Stanford University on behalf of the U.S. Department of Energy (DOE), Office of Basic Energy Sciences. We acknowledge support by the following: Human Frontier Science Program (N.D.L., M.J.B.); AMOS program within the Chemical Sciences, Geosciences, and Biosciences Division of the Office of Basic Energy Sciences, Office of Science, U.S. DOE (N.D.L., R.G.S., C.Y.H., D.S., and M.J.B.); DOE through the SLAC Laboratory Directed Research and Development Program and by Lawrence Livermore National Laboratory under Contract DE-AC52-07NA27344; the Max Planck Society for funding the development and operation of the CAMP instrument within the ASG at CFEL; the Hamburg Ministry of Science and Research and Joachim Herz Stiftung as part of the Hamburg Initiative for Excellence in Research (LEXI); the Hamburg School for Structure and Dynamics in Infection; CBST at UC under Cooperative Agreement No. PHY 0120999. Lawrence Livermore National Laboratory (LLNL) is operated by Lawrence Livermore National Security (LLC) for the U.S. DOE, National Nuclear Security Administration under Contract DE-AC52-07NA27344. Work by LLNL has been supported, in part, by University of California Laboratory Fee grant 09-LR-05-118036-BARA. We thank the staff of the LCLS for their support in carrying out these experiments. We also acknowledge support from the Swedish Research Council, the European Research Council, Knut och Alice Wallenbergs Stiftelse, and the DFG Cluster of Excellence at the Munich Centre for Advanced Photonics. The Max Planck Advanced Study Group at CFEL acknowledges technical support by R. Andritschke, K. Gärtner, O. Hälker, S. Herrmann, A. Hömke, Ch. Kaiser, K.-U. Kühnel, W. Leitenberger, D. Miessner, D. Pietschner, M. Porro, R. Richter, G. Schaller, C. Schmidt, F. Schopper, C.-D. Schröter, Ch. Thamm, A. Walenta, A. Ziegler, and H. Gorke. N.D. Loh thanks G.J. Williams for his insights.